atoms

MDPI

Article

The Double-Nozzle Technique Equipped with RF-Only Funnel and RF-Buncher for the Ion Beam Extraction into Vacuum

Victor Varentsov

Facility for Antiproton and Ion Research in Europe (FAIR), Planckstraße 1, 64291 Darmstadt, Germany; victor.varentsov@fair-center.eu

Abstract: This study is a further development of our "Proposal of a new double-nozzle technique for in-gas-jet laser resonance ionization spectroscopy" paper published in the journal *Atoms* earlier this year. Here, we propose equipping the double-nozzle technique with the RF-only funnel and RF-buncher placed in a gas-jet chamber at a 70 mm distance downstream of the double-nozzle exit. It allows for highly effective extraction into vacuum heavy ion beams, produced in two-steps laser resonance ionization in the argon supersonic jet. We explored the operation of this new full version of the double-nozzle technique through detailed gas dynamic and Monte Carlo trajectory simulations, with the results presented and discussed. In particular, our calculations showed that more than 80% of all nobelium-254 neutral atoms, extracted by argon flow from the gas-stopping cell, can then be extracted into vacuum in a form of pulsed ion beam having low transverse and longitudinal emittance.

Keywords: gas-stopping cell; supersonic gas jet; in-gas-jet laser resonance ionization spectroscopy; double-nozzle technique; RF-only funnel; RF-buncher; gas dynamic and Monte Carlo simulations

Citation: Varentsov, V. The Double-Nozzle Technique Equipped with RF-Only Funnel and RF-Buncher for the Ion Beam Extraction into Vacuum. *Atoms* **2023**, *11*, 123. https://doi.org/10.3390/atoms11100123

Academic Editor: Chengjian Lin

Received: 1 August 2023
Revised: 14 September 2023
Accepted: 20 September 2023
Published: 22 September 2023

1. Introduction

Recently, in our previous paper [1], we proposed a new double-nozzle technique for use in-gas-jet laser resonance ionization spectroscopy. The operation of this original technique was explored by means of computer experiments, which consisted in detailed gas dynamic simulations of the buffer gas flow (inside the gas-stopping cell, double-nozzle and supersonic argon gas jet) and atom-trajectory Monte Carlo simulations. The results of these computer simulations were presented and discussed in [1]. In addition, the paper [1] presents the results and discussion of similar computer simulations for the JetRIS project (see, e.g., [2,3]) that is under development at GSI and which is a typical representative of the conventional in-gas-jet technique that is in use or under development nowadays in different laboratories, as described elsewhere [4–17].

In summary, the calculation results presented in [1] show that the proposed double-nozzle technique has many advantages compared with the one used in the JetRIS setup for future high-resolution laser spectroscopic study of heaviest elements.

Readers can easily find the detailed description of the double-nozzle technique, as well as the conventional in-gas-jet technique, in, for example, [1] and many links within it.

Both experimental techniques for the laser resonance ionization spectroscopy (the proposed double-nozzle and the convention one-nozzle techniques) consist in the following.

The ions of interest, after their thermal evaporation as neutral atoms from the hot filament placed inside the gas-stopping cell in front of the nozzle, are transported by the buffer gas flow through the converging–diverging nozzle (or through the double-nozzle device, as in the case of the new technique proposed in [1]) in the gas-jet chamber.

Schematic view (from Ref. [1]) of the double-nozzle design combined with results of the gas dynamic simulation for argon velocity flow field are shown in Figure 1 for illustration.

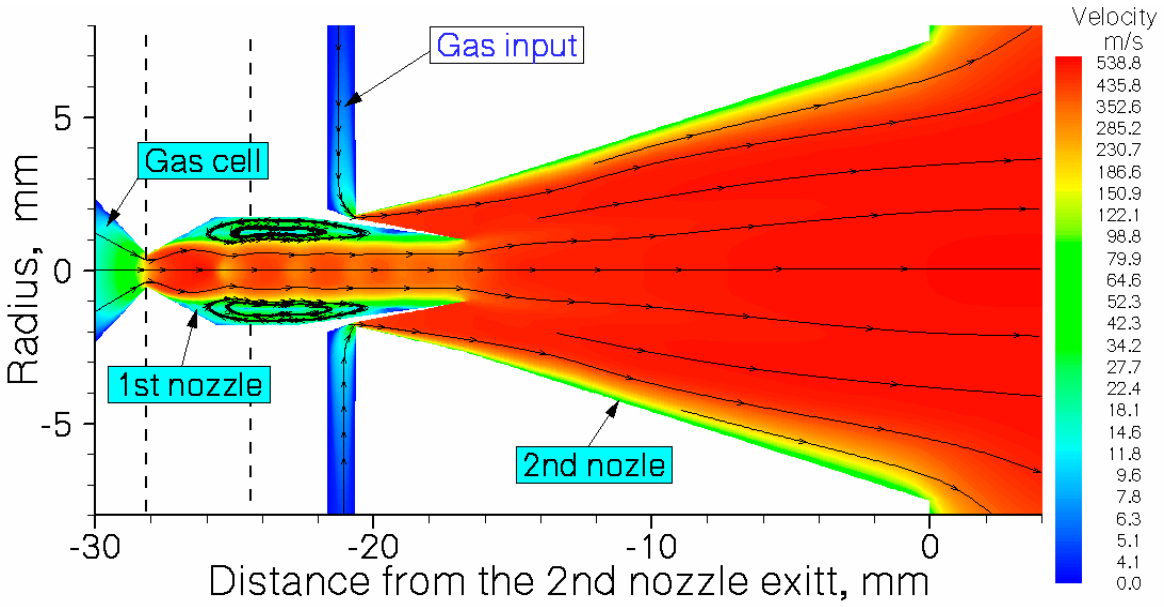

Figure 1. Schematic view of the double-nozzle design combined with results of the gas dynamic simulation for argon velocity flow field. The stagnation gas cell pressure is Pcell = 100 mbar, gas input (stagnation) pressure is P_{noz} = 81 mbar, and background pressure in the vacuum gas-jet chamber is $P_{bg} = 2.0 \times 10^{-2}$ mbar for the pumping capacity of 1300 L/s. The temperature of the gas cell and both nozzles is 296 K. Black-arrowed lines show the gas flow directions. Two black-dashed vertical lines designate a possible connection of flanges for assembling this double-nozzle device. For details of the design see Table 1 in [1].

Two lasers in cross-beam geometry perform the excitation and ionization extracted into the gas-jet chamber neutral atomic beam. (In all Monte Carlo simulations in this study, we used nobelium-254, as a representative of the heavy atoms extracted from the gas cell via argon gas flow. The goal of the JetRIS project is the study of the nuclear properties of nobelium isotopes). One laser beam (we will refer to as Laser-1) directed along the axis upstream of the gas jet direction excites atoms of interest, and the second one (we will refer to as Laser-2) directed perpendicular to the gas jet ionizes these excited atoms. The atoms ionized by the Laser-2 are transported by the gas jet through the gas-jet chamber to the entrance of the bent RFQ (e.g., S-shaped [4] or bent at 90 degrees [2–4]) and placed on the axis downstream at a 50–70 mm distance from the nozzle exit.

For instance, a description of the segmented 90° bent RFQ ion guide can be found in Section 9.1 of the detailed and good quality article [4]. This bent RFQ placed in the gas-jet chamber, shown as a 3D-schematic view in Figure 17a of [4], allows for the Laser-1 beam up to 8 mm in diameter to be inserted through the RFQ segments into the region of laser ionization.

Results of our simulations (gas dynamic + Monte Carlo) for cumulative fractions of nobelium-254 atomic beam inside the region of 8 mm in diameter (Laser-1 beam diameter) are presented in Figure 2 for different downstream distances from the GSI nozzle (in this study, we use the same definitions as in [1], e.g., “GSI nozzle” and “double-nozzle”). For the JetRIS setup operation, the stagnation gas cell pressure is P_{cell} = 100 mbar and the pumping capacity of the turbo molecular pump is 1300 L/s.

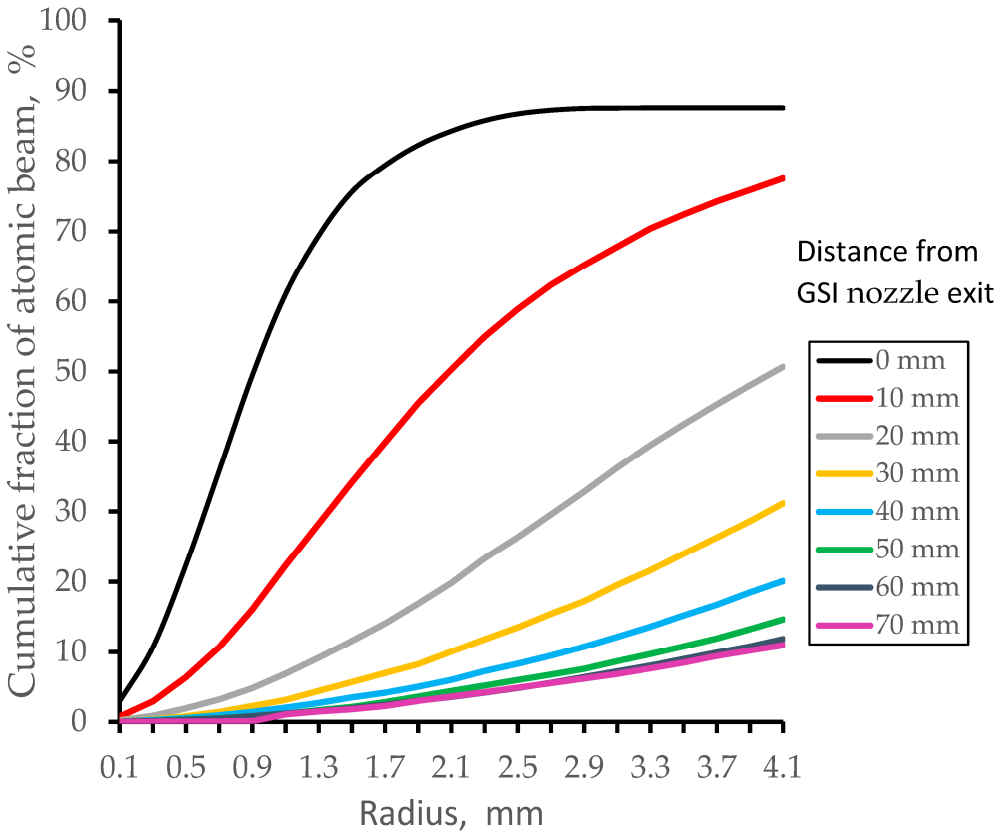

Figure 2. Simulation results for cumulative fractions of nobelium-254 atomic beam inside a diameter of 8 mm (the Laser-1's beam diameter) for different downstream distances from the GSI nozzle exit. "Cumulative fraction" here means fraction of all nobelium atoms extracted by the gas flow from the gas-stopping cell. Stagnation gas cell pressure is P_{cell} = 100 mbar; pumping capacity of the turbo molecular pump for the gas-jet chamber is 1300 L/s.

To be sure that the Laser-2 pulsed beam, with a repetition rate of 10 kHz, will ionize all nobelium atoms in a free supersonic jet, the length of the ionization zone had to be no less than 55–60 mm [2–4].

Due to the argon supersonic jet expansion (seen in Figure 4 of Ref. [1]), only nobelium atoms inside the axial region 8 mm in diameter can be excited by Laser-1. After averaging the data along the ionization region 60 mm in length in Figure 2, one can observe that only 41.9% of the total atomic beam can be ionized in the two-step laser resonance ionization process. Note that the diffusion atomic beam losses inside the nozzle were automatically included here as well.

In the case of the double-nozzle technique proposed in [1], the corresponding fraction of nobelium atomic beam that can be excited with the use of the Laser-1 beam 8 mm in diameter is 49.0%.

Unfortunately, we could not find in the literature quantitative data either on the focusing efficiency of laser-ionized heavy atom beams into the curved RFQ, or on the transmission efficiencies of these ions, first through this curved RFQ and then through the extraction RFQ placed behind the curved RFQ in the vacuum chamber (see Figure 17b in Ref. [4]).

This work is devoted to the further development of the double-nozzle technique [1]. For this reason, we suggest replacing the conventional bent RFQ in the gas-jet chamber by a simple RF-only funnel placed on the axis of the gas-jet chamber at a 70 mm distance downstream of the 2nd nozzle exit. In addition, we recommend replacing the conventional extraction RFQ (e.g., see Figure 3 in Ref. [4]) with an original compact and simple cylindrical

RF-buncher. This will allow for the fast and highly efficient ion beam extraction into vacuum and its bunching.

The idea of the RF-only funnel for ion beam extraction into vacuum was suggested for the first time in 2001 [18]. Later it was further developed and experimentally tested at Stanford University [19], ETH, Zürich [20], and the Technical University, Darmstadt [21].

A detailed description of the RF-only funnel and RF-buncher technique can be found in our recent review [22].

In Sections 3 and 4, we present the results of detailed computer simulations for the full version of the double-nozzle technique, which includes the ion beam extraction using the RF-only funnel and RF-buncher. For this purpose, we used the same software that we used in our previous work [1].

Section 5 describes the numerical investigations of the possible use of the GSI nozzle combined with the RF-only funnel and RF-buncher in the JetRIS project at GSI.

2. General Description and Main Design Parameters

The schematic view of the full version of the double-nozzle technique is shown in Figure 3. We skip a detailed description of the design of the double nozzle shown above in Figure 1 because its exact geometry is listed in Table 1 of Ref. [1].

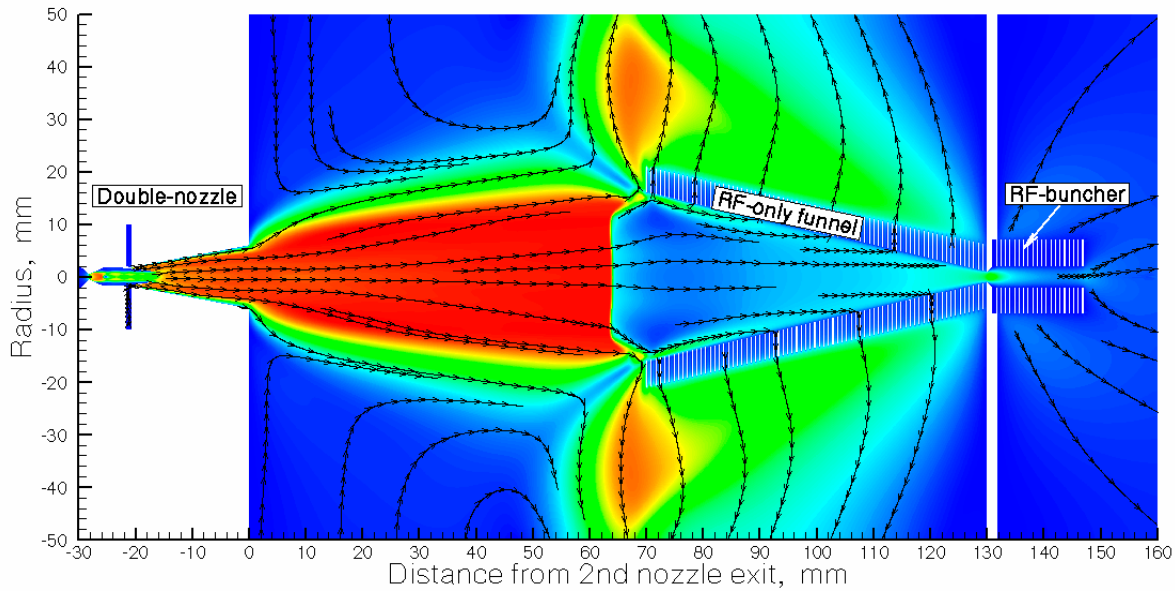

Figure 3. Schematic view of the full version of the double-nozzle technique combined with the gas dynamic simulation results for argon velocity flow field. The stagnation gas cell pressure is P_{cell} = 300 mbar, gas input (stagnation) pressure is P_{noz} = 200 mbar, and background pressure in the gas-jet chamber is $P_{bg} = 5.1 \times 10^{-2}$ mbar for the pumping capacity of 1300 L/s. The temperature of the gas cell and nozzles is 296 K. Black-arrowed lines show the gas-flow direction.

The RF-only funnel and the RF-buncher installed at the jet axis have lengths of 60 mm and 16 mm, respectively. The distance between the exit of the 2nd nozzle and the funnel entrance is 70 mm. Stainless steel funnel electrodes of 0.2 mm thickness have a shape of rings with decreasing diameters in direction to the funnel exit, but all ring-electrodes have the same width of 5 mm (the difference between the outer and inner rings' radii). Electrodes of the RF-buncher are similar to electrodes of the RF-only funnel, but have a cylindrical geometry, where all electrodes have a constant inner diameter of 4 mm.

Each ring-electrode has two supporting legs of approximately 3–6 mm width for their assembling into the funnel and buncher stacks on the supporting rods. The assembly of electrodes into the funnel and buncher can be performed similarly as described in detail in [10], in particular, as shown in their photographs in Figure 4.

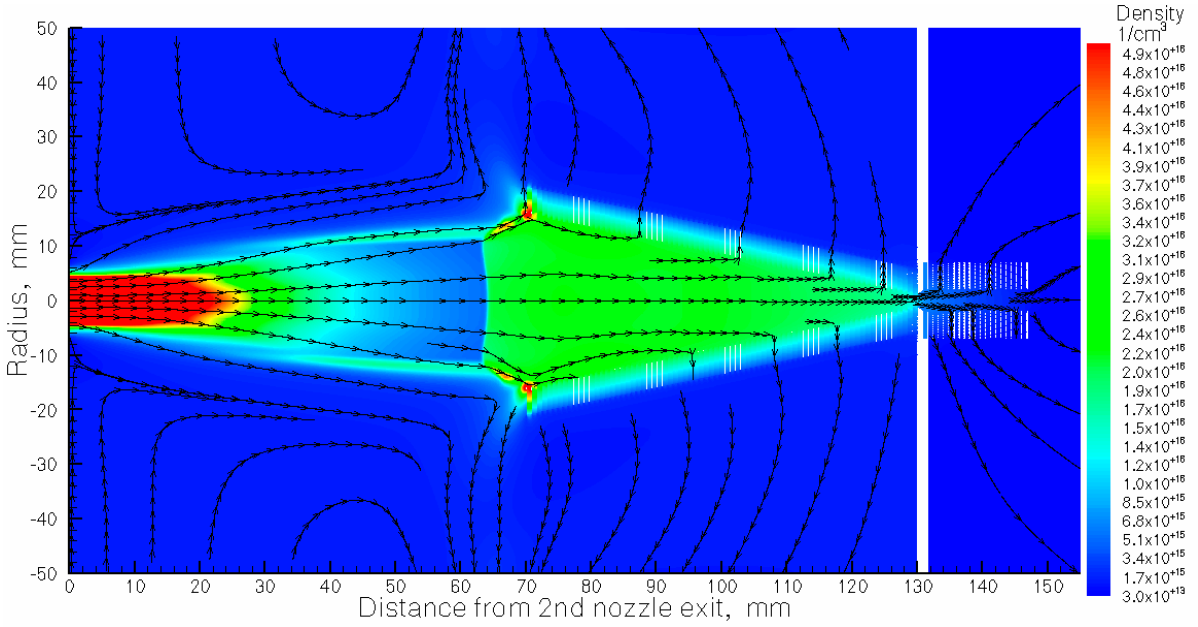

Figure 4. Results of the gas dynamic simulation for argon density flow field. The stagnation gas-cell pressure P_{cell} = 300 mbar, gas input (stagnation) pressure P_{noz} = 200 mbar, and background pressure in the gas-jet chamber $P_{bg} = 5.1 \times 10^{-2}$ mbar for the pumping capacity of 1300 L/s. The temperature of the gas cell and nozzles is 296 K. Black-arrowed lines show the gas flow direction.

Main design parameters of the RF-only funnel and RF-buncher listed in Table 1.

Table 1. Main design parameters of the RF-only funnel and RF-buncher.

	Rf-Only Funnel	RF-Buncher
Entrance aperture diameter (mm)	32	4
Exit aperture diameter (mm)	2	4
Electrode thickness (mm)	0.2	0.2
Inter-electrode spacing (mm)	0.6	0.6
Number of electrodes	75	20

Taking into account that the exit aperture of the RF-only funnel has a diameter of 2 mm, the Laser-1 beam inserted through this aperture into the gas-jet chamber must have some small divergence in order to cover the nobelium atoms inside the supersonic jet in the region of their ionization. It can be realized by optics, when the Laser-1 beam has focused at approximately a 2 mm distance downstream of the RF-buncher exit and then diverged and passed through the RF-buncher and RF-only funnel with a half-divergence angle of 3.2°. In this case, the Laser-1 beam will have a diameter of 12 mm at a 40 mm downstream distance from the 2nd nozzle exit. The results of the Monte Carlo simulations presented below in Section 3 definitely show that this Laser-1 beam geometry is well suited for excitation of the nobelium atomic beam in the supersonic jet.

The pulsed ion beam extracted from the RF-buncher into a vacuum of 10^{-3}–10^{-4} mbar with low transverse and longitudinal emittance can be easily bent 90° using a standard Quadrupole deflector, e.g., as shown in Figure 1 of Ref. [6].

3. Results of Gas Dynamic Simulations

The results of the gas dynamic simulations for eight combinations of gas stagnation pressures in the gas cell (P_{cell}) and in the double-nozzle (P_{noz}) are listed in Table 2.

Table 2. Results of gas dynamic simulations for the gas flow rates through the nozzles at pumping capacity of the gas-jet chamber of 1300 L/s.

Calculation Variant	**#1**	**#2**	**#3**	**#4**	**#5**	**#6**	**#7**	**#8**
Stagnation pressure P_{cell} (mbar)	100	100	200	200	200	300	300	300
Stagnation pressure P_{noz} (mbar)	200	300	100	200	300	100	200	300
Background pressure in gas-jet chamber P_{bg} (mbar)	0.033	0.045	0.03	0.042	0.054	0.039	0.051	0.063
Total gas flow rate Q_{tot} (mbar L/s)	42.8	58.4	38.8	54.4	70	50.4	66	81.6
Gas flow rate through funnel exit into vacuum Q_{vac} (mbar L/s)	0.154	0.435	0.053	0.172	0.538	0.11	0.245	0.432
Flow rate ratio Q_{tot}/Q_{vac}	278	134	732	316	112	458	269	189

Results of the gas dynamic simulation of argon gas density, temperature, Mach number and velocity flow fields are presented in the next four Figures for the calculation variant #7 (see Table 2).

Of course, we could present pictures with results of gas dynamic simulations for each calculation variant listed in Table 2, but we decided not to overload the text of this paper with many similar, in principle, graphic figures.

In Figures 4–8 one can clearly see the effect of a strong interaction of the supersonic gas jet with the RF-only funnel, when the supersonic gas flow passing through the direct shockwave (or how it is sometimes called—a Mach disk) are converted into subsonic gas flow. In a sense, we can say that this RF-only funnel works as a "killer" of the supersonic gas jet.

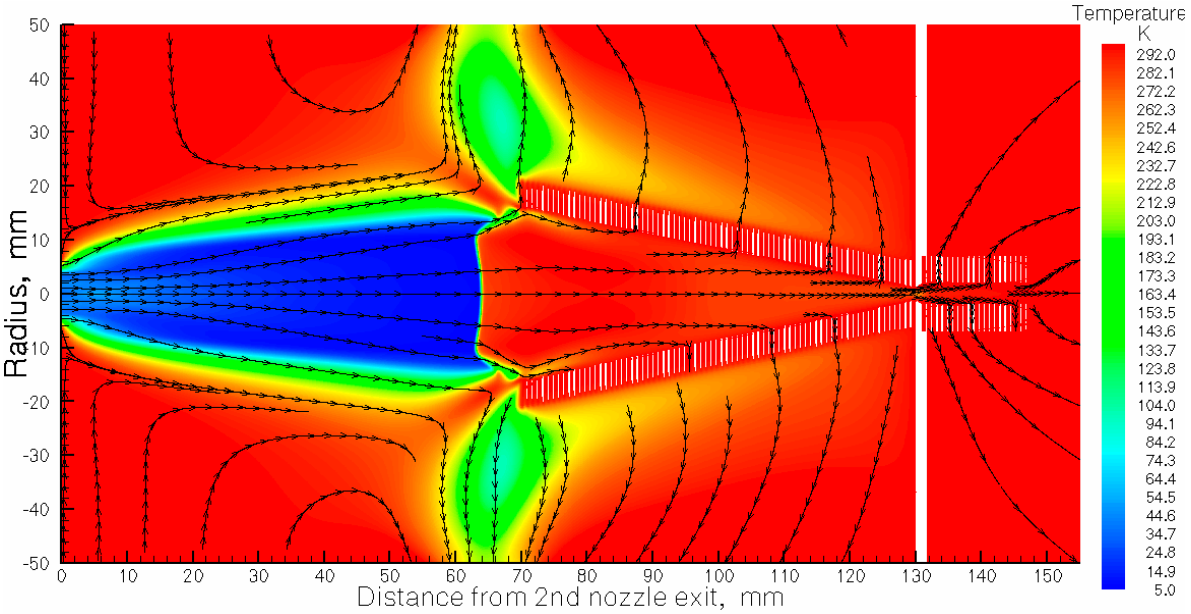

Figure 5. Results of the gas dynamic simulation for the argon temperature flow field. The stagnation gas cell pressure P_{cell} = 300 mbar, gas input (stagnation) pressure P_{noz} = 200 mbar, and background pressure in the gas-jet chamber $P_{bg} = 5.1 \times 10^{-2}$ mbar for the pumping capacity of 1300 L/s. The temperature of the gas cell and nozzles is 296 K. Black-arrowed lines show the gas flow direction.

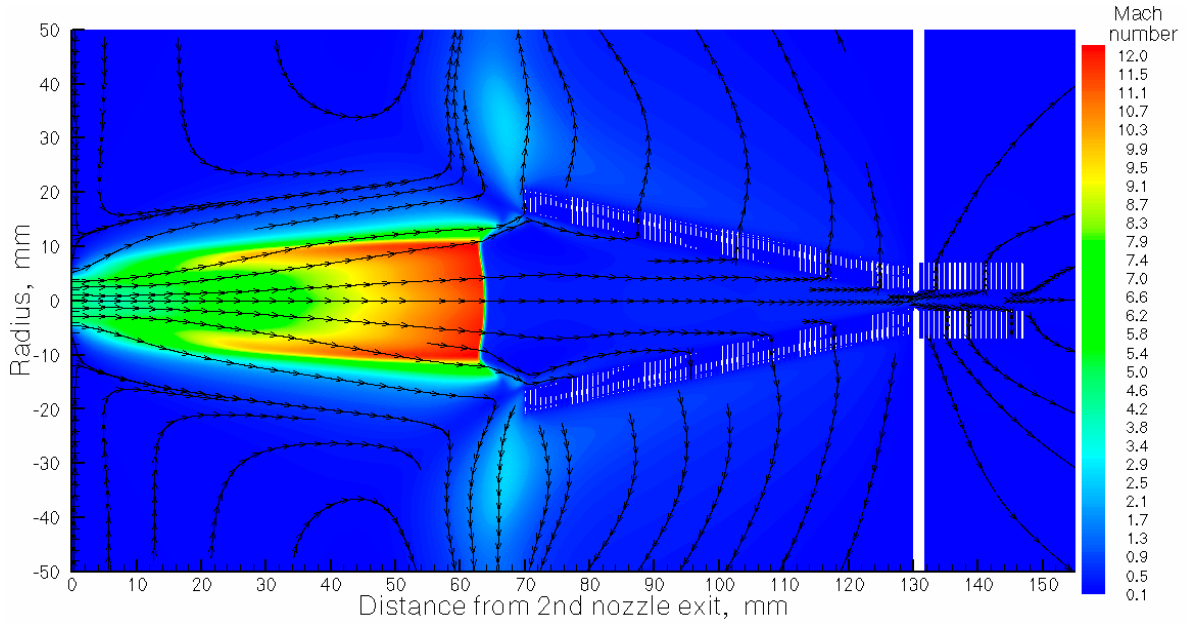

Figure 6. Results of the gas dynamic simulation for the argon Mach number flow field. The stagnation gas cell pressure P_{cell} = 300 mbar, gas input (stagnation) pressure P_{noz} = 200 mbar, and background pressure in the gas-jet chamber $P_{bg} = 5.1 \times 10^{-2}$ mbar for the pumping capacity of 1300 L/s. The temperature of the gas cell and nozzles is 296 K. Black-arrowed lines show the gas flow direction.

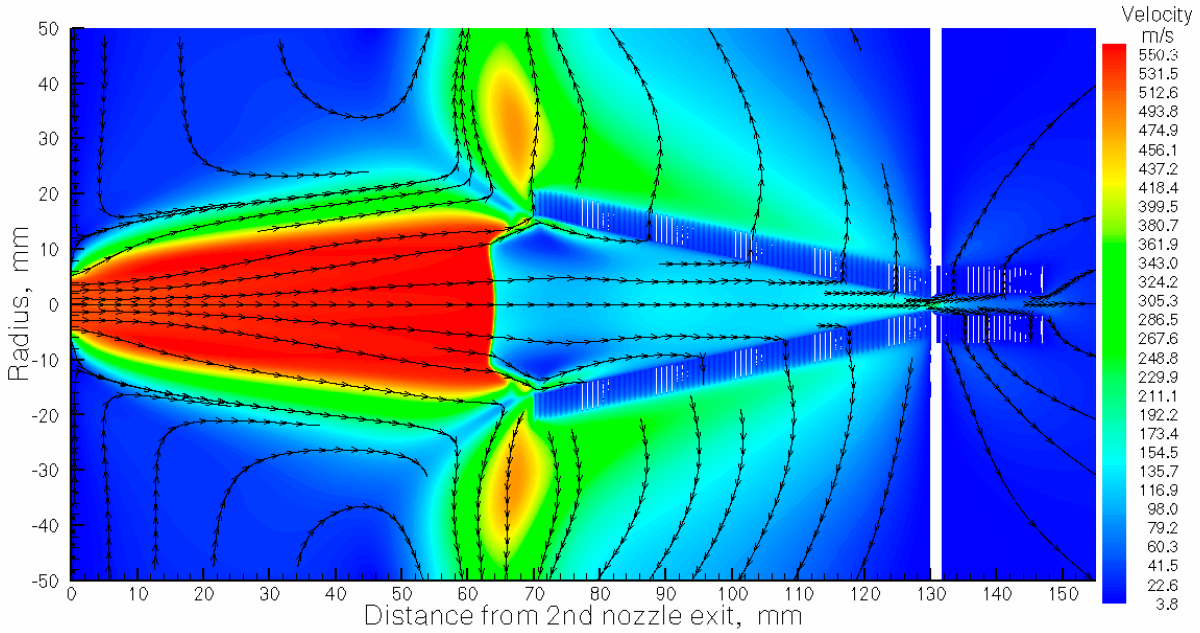

Figure 7. Results of the gas dynamic simulation for the argon velocity flow field. The stagnation gas cell pressure P_{cell} = 300 mbar, gas input (stagnation) pressure P_{noz} = 200 mbar, background pressure in the gas-jet chamber $P_{bg} = 5.1 \times 10^{-2}$ mbar for the pumping capacity of 1300 L/s. The temperature of the gas cell and nozzles is 296 K. Black-arrowed lines show the gas flow direction.

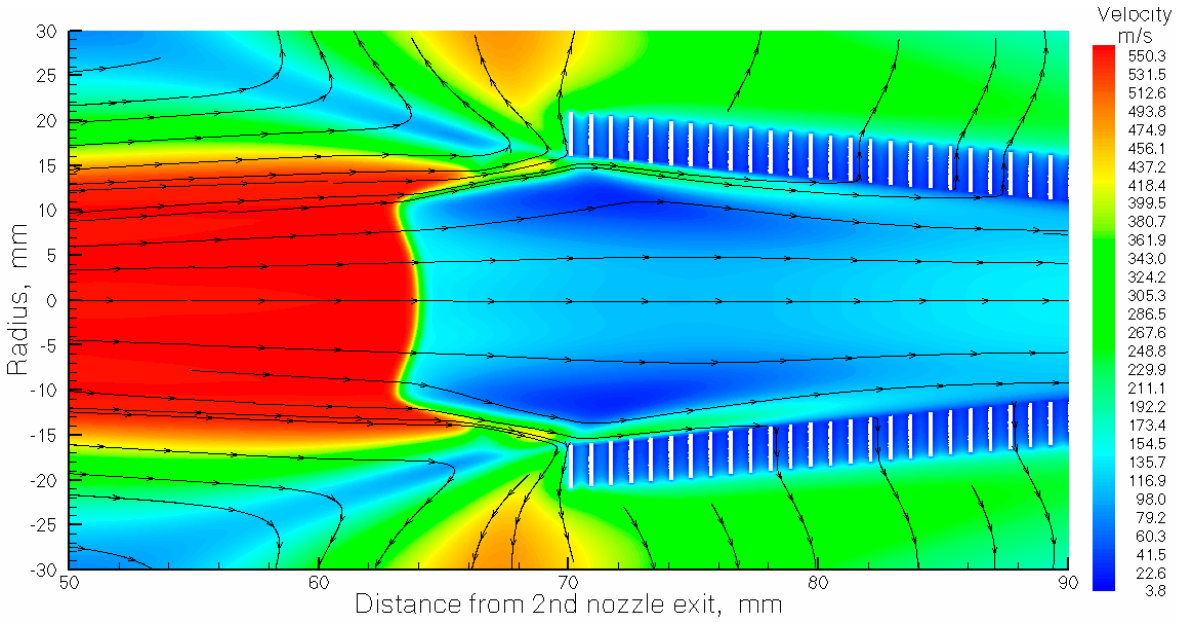

Figure 8. Results of the gas dynamic simulation for the argon velocity flow field in the region of the RF-only funnel entrance. This is part of Figure 7, shown in closeup view.

4. Results of Monte Carlo Trajectory Simulations

Results of simulations for the atomic beam radius (90% level) for different distances from the 2nd nozzle exit and for eight calculation variants are listed in Table 3. The gas stagnation and background pressures for each calculation variant is listed in Table 2 above.

Table 3. Results of Monte Carlo simulations for the atomic beam radius (90% level) at different downstream distances from the 2nd nozzle exit for eight calculation variants. Radius values in (mm). Number of calculated atoms is 10,000 for each variant.

Calculation Variant	#1	#2	#3	#4	#5	#6	#7	#8
0 mm	2.0	2.0	2.14	2.17	2.08	2.2	2.2	2.23
10 mm	2.25	2.35	2.6	2.36	2.29	2.62	2.36	2.33
20 mm	2.84	4.35	3.91	3.1	2.74	4.09	3.22	2.89
30 mm	3.83	4.95	5.6	4.36	3.69	5.99	4.54	3.98
40 mm	5.1	6.6	7.6	5.69	4.84	7.99	6.02	5.26
50 mm	6.4	8.15	9.5	7.32	6.07	9.98	7.7	6.57
60 mm	7.8	10.5	11.4	8.78	7.32	11.8	9.35	7.96

As an illustration of the data in Table 3, Figure 9 shows the calculated cumulative radial distributions of the nobelium-254 atomic beam at different downstream distances from the 2nd nozzle exit for the calculation variant #7.

The diverging Laser-1 beam has a radius of 6 mm at a 40 mm distance from the 2nd nozzle exit. Therefore, by using the data in Figure 9, we conclude that the Laser-1 beam overlaps 87.3% of all atoms extracted from the gas-stopping cell by the gas flow and, as a result, they can be ionized in the process of two-step resonance laser ionization.

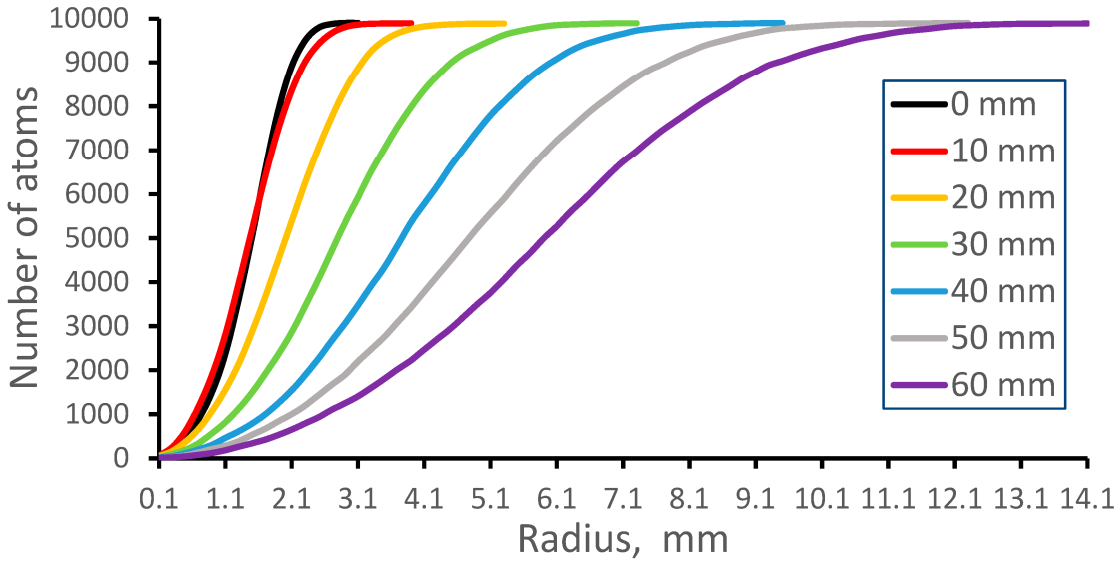

Figure 9. Results of Monte Carlo trajectory simulations for cumulative radial distributions of the nobelium-254 atomic beam at different downstream distances from the 2nd nozzle exit for the calculation variant #7. The number of calculated atoms is 10,000 for each distance.

Results of Monte Carlo simulations for atomic beam longitudinal and radial velocity spreads (FWHM) as a function of the distance downstream from the 2nd nozzle exit are listed in Tables 4 and 5, respectively. As an illustration of the data in Tables 4 and 5, Figures 10 and 11 show calculated longitudinal and radial velocity distributions of the nobelium-254 atomic beam for the calculation variant #7.

Table 4. Results of Monte Carlo trajectory simulations for atomic beam longitudinal velocity spread (FWHM) in m/s as a function of the downstream distance from the 2nd nozzle exit for different calculation variants. The data are averaged in the radial plane for the total beam. Number of calculated atoms is 10,000 for each calculation variant.

Calculation Variant	#1	#2	#3	#4	#5	#6	#7	#8
0 mm	97.6	95.7	94.5	90.8	91.2	93.6	95.0	86.1
10 mm	88.7	89.4	78.0	87.3	87.6	90.4	85.0	81.2
20 mm	60.1	65.0	65.5	73.4	77.6	66.5	71.4	73.7
30 mm	64.0	59.9	56.6	62.9	64.4	54.2	57.1	63.7
40 mm	55.0	50.8	52.4.	54.5	54.2	47.2	51.1	59.4
50 mm	50.7	47.7	44.6	47.0	48.5	43.5	45.0	45.5
60 mm	46.8	47.8	43.2	41.6	44.6	41.3	43.4	42.6

Table 5. Results of Monte Carlo trajectory simulations for atomic beam radial velocity spread (FWHM) in m/s as a function of the downstream distance from the 2nd nozzle exit for different calculation variants. The data are averaged in the radial plane for the total beam diameter. Number of calculated atoms is 10,000 for each calculation variant.

Calculation Variant	#1	#2	#3	#4	#5	#6	#7	#8
0 mm	63.7	45.2	52.5	61.5	63.2	64.6	59.3	53.5
10 mm	70.9	49.1	72.4	60.7	57.2	69.1	68.1	58.6
20 mm	59.4	53.2	72.2	65.1	61.1	78.3	64.0	60.9
30 mm	62.3	57.3	86.0	67.7	61.2	83.3	64.5	62.0
40 mm	69.3	55.5	78.0	71.2	64.2	69.4	66.3	63.3
50 mm	66.3	55.2	81.6	67.9	64.9	70.6	60.0	62.6
60 mm	67.0	52.3	82.7	73.3	63.0	71.0	56.2	64.6

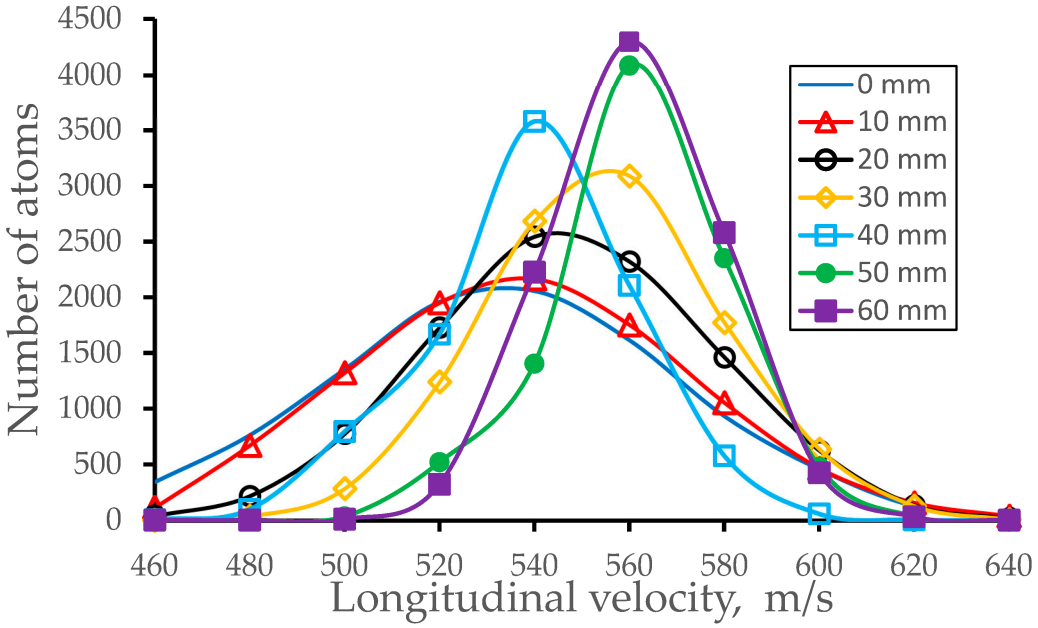

Figure 10. Results of Monte Carlo trajectory simulations for atomic beam longitudinal velocity distributions for different distances from the 2nd nozzle exit for the calculation variant #7. The data are averaged in the radial plane for the total beam. Number of calculated atoms is 10,000 for each distance.

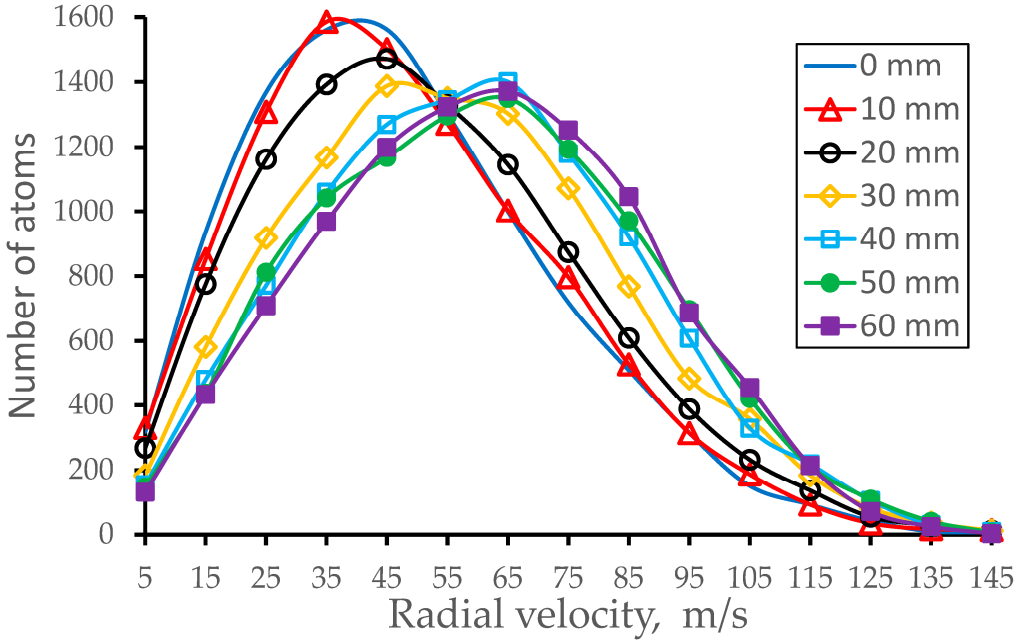

Figure 11. Results of Monte Carlo trajectory simulations for atomic beam radial velocity distributions for different distances from the 2nd nozzle exit for the calculation variant #7. The data are averaged in the radial plane for the total beam. Number of calculated atoms is 10,000 for each distance.

Table 6 presents the results of Monte Carlo simulations for the atomic beam time of flight (μsec) starting from the gas cell nozzle throat as a function of the downstream distance from the 2nd nozzle exit for eight calculation variants. It is clear that the length of the ionization zone of 60 mm is enough to ionize all Laser-1-excited nobelium atoms by the pulsed Laser-2 beam with the repetition rate of 10 kHz and enough diameter size. We

assume that the efficiency of ionization of nobelium atoms is equal to 100% when they are simultaneously exposed to both lasers.

Table 6. Results of Monte Carlo trajectory simulations for the atomic beam time of flight in μsec starting from the gas cell nozzle throat as a function of the downstream distance from the 2nd nozzle exit for eight calculation variants. The data are averaged in the radial plane for the total beam diameter. Number of calculated atoms is 10,000 for each calculation variant.

Calculation Variant	#1	#2	#3	#4	#5	#6	#7	#8
0 mm	68	68	64	64	64	63	63	63
10 mm	88	88	86	84	84	82	82	82
20 mm	108	108	104	103	102	101	101	101
30 mm	125	124	124	121	121	120	120	120
40 mm	144	142	142	140	140	138	138	138
50 mm	162	162	162	158	157	157	155	155
60 mm	180	180	180	176	176	175	174	174

The RF frequency and voltages applied to the RF-only funnel and RF-buncher electrodes, which we used in Monte Carlo simulations, are listed in Table 7.

Table 7. RF frequency and RF amplitude (peak-to-peak) applied to the extraction RF-only funnel and RF-buncher. Extraction DC field = −10 V/cm.

	RF-Only Funnel	RF-Buncher
RF-amplitude [V_{pp}]	100	100
RF-frequency [MHz]	5	5
Rf-funnel-RFbuncher DC bias	-	−0.8 V
DC potential gradient	-	−0.08 V

For instance, the calculated capacitance of this RF-only funnel is equal to 0.235 nF, which corresponds to a capacitive reactance of 135 ´Ω at operating frequency of 5 MHz.

Main calculated characteristics of the extracted-pulsed nobelium ion beam are listed in Tables 8 and 9.

Table 8. Results of Monte Carlo simulations for fraction of ions in nobelium-254 beam at RF-only funnel entrance and total ion beam extraction efficiency into vacuum for eight calculation variants. The number of calculated ions is 10,000 for each variant.

Calculation Variant	#1	#2	#3	#4	#5	#6	#7	#8
Fraction of ions in nobelium beam at RF-only funnel entrance (%)	89.6	82.3	76.9	85.7	91.0	74.9	83.5	88.2
Total ion beam extraction efficiency into vacuum (%)	69.7	52.6	46.8	79.5	89.0	66.1	81.2	87.4

Table 9. Results of Monte Carlo trajectory simulations for main parameters of the extracted pulsed nobelium ion beam for eight calculation variants. Number of calculated ions is 10,000 for each variant.

Calculation Variant	#1	#2	#3	#4	#5	#6	#7	#8
Longitudinal (90%) energy spread (eV)	0.29	1.1	0.43	0.42	0.62	0.46	0.45	0.59
Bunch time (90%) width (μs)	9	9	9	9	9	9	9	9.4
Longitudinal emittance (90%) (eV μs)	2.6	9.9	3.8	3.8	5.6	4.1	4.0	5.6
Beam radius (90%) (mm)	1.85	1.93	1.90	1.88	1.88	1.90	1.92	1.95
Transverse (90%) energy spread (eV)	0.12	0.21	0.18	0.18	0.17	0.23	0.16	0.17
Normalized transverse emittance (90%) (π·mm·mrad·[eV]$^{1/2}$)	224	156.1	292	289	309.8	321	336	310

We would like to emphasize that the values of total ion beam extraction efficiency into vacuum in Table 8 include both diffusion losses of atoms inside the double-nozzle and ion losses inside the RF-only funnel. The transmission efficiency of ions through the RF-buncher is close to 100% for all calculation variants. In other words, the total ion beam extraction efficiencies here are the ratio of the number of extracted into vacuum nobelium ions, obtained in result of two-stage resonant laser ionization, to the number of neutral nobelium atoms extracted by the gas flow from the gas cell.

5. Perspectives of Using the RF-Only Funnel and RF-Buncher for the JetRIS Project at GSI

To check the efficiency of the possible use of the described above RF-only funnel and RF-buncher in the JetRIS project with the GSI nozzle, we performed gas dynamic and Monte Carlo simulations, similar to those presented above for the double-nozzle technique.

The design parameters and operation conditions of RF-only funnel and RF-buncher used in these simulations are the same as listed in Tables 1 and 7, respectively.

5.1. Results of Gas Dynamic Simulations

Results of gas dynamic simulations for the GSI nozzle at two gas cell stagnation pressures listed in Table 10.

Table 10. Results of gas dynamic simulations for the gas flow rates through the GSI nozzle at pumping capacity of the gas-jet chamber of 1300 L/s.

Stagnation Pressure P_{cell}	**200 Mbar**	**300 Mbar**
Background pressure in gas-jet chamber P_{bg} (mbar)	0.0178	0.0267
Total gas flow rate Q_{tot} (mbar L/s)	23.2	34.8
Gas flow rate through funnel exit into vacuum Q_{vac} (mbar L/s)	0.05	0.271
Flow rate ratio Q_{tot}/Q_{vac}	464	128

Figure 12 shows the results of the gas dynamic simulation for the gas velocity flow field in the region of the RF-only funnel entrance for boundary conditions listed in Table 10 for the stagnation gas pressure P_{cell} = 300 mbar. This Figure demonstrates a clear difference in detailed structure of the supersonic jet flowing out of the GSI nozzle compared to that for the case of the double-nozzle operation shown in Figure 8 for the calculation variant #7 (see Table 2).

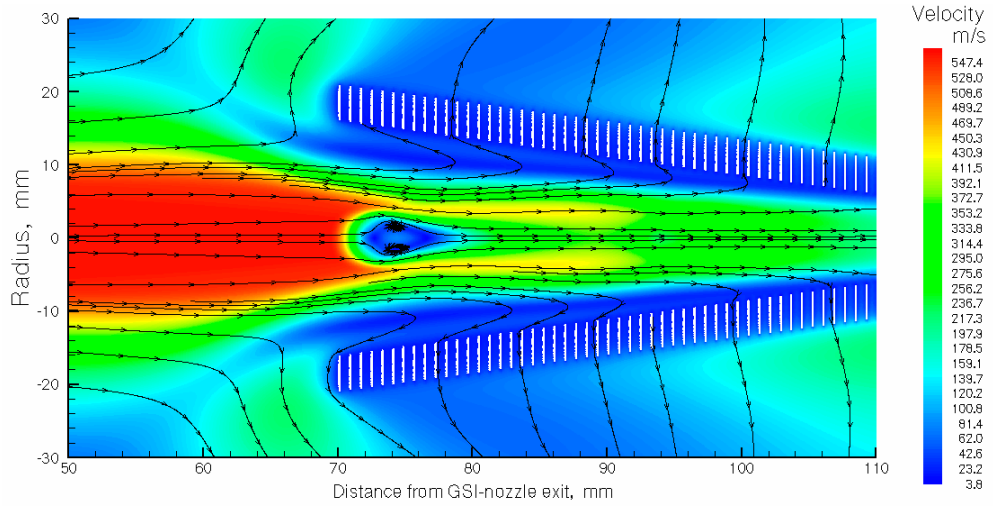

Figure 12. Results of the gas dynamic simulation for argon velocity flow field in the region of the RF-only funnel entrance for the GSI nozzle operating at P_{cell} = 300 mbar and pumping capacity in the gas-jet chamber of 1300 L/s.

5.2. Results of Monte Carlo Simulations

Tables 11 and 12 present the results of Monte Carlo simulations for nobelium-254 atomic beam parameters for different downstream distances from the GSI nozzle exit.

Table 11. Results of simulations for nobelium-254 atomic beam parameters for different downstream distances from the GSI nozzle exit. Stagnation pressure is P_{cell} = 200 mbar, background pressure is P_{bg} = 0.0179 mbar, and the nozzle temperature is T_0 = 296 K. Number of calculated ions is 10,000 for each distance.

Distance from GSI Nozzle Exit (mm)	**0**	**10**	**20**	**30**	**40**	**50**	**60**
Beam radius (90%) (mm)	1.68	3.8	6.68	9.27	11.06	12.4	13.12
Longitudinal velocity spread (FWHM) (m/s)	91.2	59.0	43.3	40.2	40.6	44.1	56.0
Radial velocity spread (FWHM) (m/s)	65.1	99.8	99.2	85.0	58.0	51.0	59.4
Time of flight (μs)	44	60	80	96	116	132	152

Table 12. Results of simulations for nobelium-254 atomic beam parameters for different downstream distances from the GSI nozzle exit. Stagnation pressure is P_{cell} = 300 mbar, background pressure is P_{bg} = 0.0268 mbar, and the nozzle temperature is T_0 = 296 K. Number of calculated ions is 10,000 for each distance.

Distance from GSI Nozzle Exit (mm)	**0**	**10**	**20**	**30**	**40**	**50**	**60**
Beam radius (90%) (mm)	1.67	3.6	6.1	8.4	10.3	11.8	11.8
Longitudinal velocity spread (FWHM) (m/s)	84.3	55.1	51.4	47.8	38.1	40.0	43.6
Radial velocity spread (FWHM) (m/s)	56.9	95.9	97.2	80.5	71.3	50.7	44.0
Time of flight (μs)	44	60	80	96	116	132	152

Table 13 presents the results of Monte Carlo simulations for total nobelium-254 ion beam extraction efficiencies into vacuum for different stagnation gas cell pressures P_{cell}.

Table 13. Results of Monte Carlo simulations for total nobelium-254 ion beam extraction efficiencies for different stagnation gas pressures P_{cell}. The number of calculated ions is 10,000 for each variant.

Stagnation Pressure P_{cell}	**200 Mbar**	**300 Mbar**
Fraction of ions in nobelium beam at FR-only funnel entrance (%)	64.2	64.9
Total ion beam extraction efficiency into vacuum (%)	16.8	35.4

Important note. If participants of the JetRIS project ever decide to experimentally test the functionality of the described RF-only funnel and RF-buncher installed into their present setup with GSI nozzle, they should not be surprised if at P_{cell} = 100 mbar they would not see any ions extracted from the RF-buncher into vacuum.

The point is that at this stagnation pressure in the gas cell, the supersonic free jet is not powerful enough, and the viscous subsonic gas flow transporting ions is almost completely "killed"(or strongly decelerated) inside the RF-only funnel. Thus, most of the ions are lost, the gas flow rate into the RF-buncher turns out to be less than 0.01 mbar l/s, and this is insufficient for efficient ion-beam bunching. We performed the simulations for this pressure (Pcell = 100 mbar) as well, but we decided not to include these results in the article.

6. Discussion and Outlook

In Section 2 of the article, we presented the description of the suggested full version of the double-nozzle technique, shown as a schematic view in Figure 3. Main design parameters of the RF-only funnel and RF-buncher listed in Table 1. The compact RF-only funnel of 60 mm length and RF-buncher of 16 mm length have a simple design, can be easily manufactured and installed on the axis of the gas-jet chamber at a 70 mm downstream distance from the exit of the double-nozzle.

Results of the gas dynamic simulations for eight combinations of gas stagnation pressures in the gas cell (Pcell) and in the double-nozzle (Pnoz) are presented in Section 3. The graphic description of the supersonic and subsonic gas flow structure (flow fields of gas density, temperature, Mach number and velocity) are shown for the calculation variant #7 (see Table 2) in Figures 4–8. Here, one can clearly see in the jet a direct shock wave approximately 20 mm in diameter, which appears in front of the RF-only funnel due to a strong interaction of the supersonic gas jet with this funnel. The supersonic gas jet passing through this direct shockwave is converted into subsonic gas flow, and it greatly helps to dramatically decrease the gas load into the vacuum chamber with the RF-buncher (for details, see Q_{vac} values in Table 2).

Results of many Monte Carlo simulations are presented in Section 4 in the form of tables and graphics. In particular, the values of total ion beam extraction efficiency into vacuum are listed in Table 8 for all eight calculation variants. Main parameters of the extracted bunched nobelium ion beam, including values of longitudinal and normalized transverse emittance, for eight calculation variants can be found in Table 9.

In order to find out how effective is the use of the RF-only funnel and RF-buncher even in case of their use for conventional technology of in-gas-jet laser resonance spectroscopy (e.g., in the setup of the JetRIS project at GSI), we performed similar gas dynamic + Monte Carlo simulations. These results are presented in Section 5 for the GSI nozzle operation at Pcell values of 200 mbar and 300 mbar and at the pumping speed of 1300 L/s.

There is an impressive difference between gas flow structure shown in Figure 12 and the one shown in Figure 7 for the double-nozzle technique (variant #7 in Table 2).

It is also interesting to note that the gas flow rate through funnel exit into vacuum is Q_{vac} = 0.05 mbar L/s for the case of P_{cell} = 200 mbar (see Table 10) in a factor of 5.4 less than this value for the case of P_{cell} = 300 mbar. At first glance, this looks great because with such a small gas load into the vacuum chamber, where the RF-buncher is located, it is enough to use a vacuum pump with a capacity of 100 L/s to maintain a vacuum in this chamber at a level of 5×10^{-4} mbar. On the other hand, the total efficiency of ion beam extraction into vacuum at P_{cell} = 200 mbar turns out to be only 16.8% (see Table 13), which is 2.1 times less than this value for the case of P_{cell} = 300 mbar. That is why the variant of P_{cell} = 300 mbar is, in our opinion, more preferable for experiments with radioactive elements. For instance, the authors of [2] share the same opinion, writing in their abstract: "In view of the low production rates of the heaviest elements, a high total efficiency is a crucial requirement for any experimental setup to be used in on-line experiments".

In this respect, our double-nozzle technique also has great advantages over the conventional in-gas-jet laser resonance ionization technique [2–4], even when they both use the RF-only funnel and RF-buncher. This assertion is confirmed by the results of our above-presented calculations because the total extraction efficiency of the nobelium-254 ions into vacuum is 81.2% (see variant #7 in Table 8), which is 2.3 times higher than the one for the Pcell = 300 mbar variant in Table 13.

Funding: This research received no external funding.

Data Availability Statement: The data presented in this study are available upon request from the corresponding author.

Conflicts of Interest: The author declares no conflict of interest.

References

1. Victor, V. Proposal of a New Double-Nozzle Technique for In-Gas-Jet Laser Resonance Ionization Spectroscopy. *Atoms* **2023**, *11*, 88. [CrossRef]
2. Raeder, S.; Block, M.; Chhetri, P.; Ferrer, R.; Kraemer, S.; Kron, T.; Laatiaoui, M.; Nothhelfer, S.; Schneider, F.; Van Duppen, P.; et al. A gas-jet apparatus for high-resolution laser spectroscopy on the heaviest elements at SHIP. *Nucl. Instrum. Methods Phys. Res. B* **2020**, *463*, 272–276. [CrossRef]
3. Münzberg, D.; Block, M.; Claessens, A.; Ferrer, R.; Laatiaoui, M.; Lantis, J.; Nothhelfer, S.; Raeder, S.; Van Duppen, P. Resolution Characterizations of JetRIS in Mainz Using 164Dy. *Atoms* **2022**, *10*, 57. [CrossRef]

4. Kudryavtsev, Y.; Ferrer, R.; Huyse, M.; Van den Bergh, P.; Van Duppen, P. The in-gas-jet laser ion source: Resonance ionization spectroscopy of radioactive atoms in supersonic gas jets. *Nucl. Instrum. Methods Phys. Res. B* **2013**, *297*, 7–22. [CrossRef]
5. Yang, X.F.; Wang, S.J.; Wilkins, S.G.; Ruiz, R.G. Laser Spectroscopy for the Study of Exotic Nuclei. *Prog. Part. Nucl. Phys.* **2023**, *129*, 104005. [CrossRef]
6. Block, M.; Giacoppo, F.; Heßberger, F.P.; Raeder, S. Recent progress in experiments on the heaviest nuclides at SHIP. *La Riv. Del Nuovo C.* **2022**, *45*, 279–323. [CrossRef]
7. Van Duppen, P. In-Gas Jet Laser Ionization Spectroscopy of Heavy Elements. Available online: https://www.psi.ch/sites/default/files/import/ltp/ThursdayColloquiaEN/2018_11_Laser_spectroscopy_Heavy_Elements_Piet_Van_Duppen.pdf (accessed on 31 July 2023).
8. Ferrer, R.; Barzakh, A.; Bastin, B.; Beerwerth, R.; Block, M.; Creemers, P.; Grawe, H.; de Groote, R.; Delahaye, P.; Fle'chard, X.; et al. Towards high-resolution laser ionization spectroscopy of the heaviest elements in supersonic gas jet expansion. *Nat. Commun.* **2017**, *8*, 14520. [CrossRef] [PubMed]
9. Ferrer, R.; Verlinde, M.; Verstraelen, E.; Claessens, A.; Huyse, M.; Kraemer, S.; Kudryavtsev, Y.; Romans, J.; Van den Bergh, P.; Van Duppen, P.; et al. Hypersonic nozzle for laser-spectroscopy studies at 17 K characterized by resonance-ionization-spectroscopy-based flow mapping. *Phys. Rev. Res.* **2021**, *3*, 043041. [CrossRef]
10. Sels, S.; Ferrer, R.; Dockx, K.; Buitrago, C.G.; Huyse, M.; Kudryavtsev, Y.; Kraemer, S.; Raedera, S.; Van Den Bergh, P.; Van Duppen, P.; et al. Design and commissioning of an ion guide system for In-Gas Laser Ionization and Spectroscopy experiments. *Nucl. Instrum. Methods Phys. Res. B* **2020**, *463*, 148–153. [CrossRef]
11. Romans, J.; Ajayakumar, A.; Authier, M.; Boumard, F.; Caceres, L.; Cam, J.-F.; Claessens, A.; Damoy, S.; Delahaye, P.; Desrues, P.; et al. First Offline Results from the S^3 Low-Energy Branch. *Atoms* **2022**, *10*, 21. [CrossRef]
12. Hirayama, Y.; Watanabe, Y.X.; Schury, P.; Mukai, M.; Choi, H.; Ahmed, M.; Kakiguchi, Y.; Oyaizu, M.; Wada, M.; Miyatake, H. In-gas-jet laser ionization spectroscopy at KISS. *RIKEN Accel. Prog. Rep.* **2019**, *52*, 1.
13. Hirayama, Y.; Watanabe, Y.X.; Mukai, M.; Ahmed, M.; Ishiyama, H.; Jeong, S.C.; Kakiguchi, Y.; Kimura, S.; Moon, J.Y.; Oyaizu, M.; et al. Nuclear spectroscopy of r-process nuclei using KEK Isotope Separation System. *J. Phys. Conf. Ser.* **2020**, *1643*, 012138. [CrossRef]
14. Kudryavtsev, Y.; Creemers, P.; Ferrer, R.; Granados, C.; Gaffney, L.P.; Huyse, M.; Mogilevskiy, E.; Raeder, S.; Sels, S.; Van den Bergh, P.; et al. A new in-gas-laser ionization and spectroscopy laboratory for off-line studies at KU Leuven. *Nucl. Instrum. Methods Phys. Res. B* **2016**, *376*, 345–352. [CrossRef]
15. Zadvornaya, A.; Creemers, P.; Dockx, K.; Ferrer, R.; Gaffney, L.P.; Gins, W.; Granados, C.; Huyse, M.; Kudryavtsev, Y.; Laatiaoui, M.; et al. Papadakis Characterization of Supersonic Gas Jets for High-Resolution Laser Ionization Spectroscopy of Heavy Elements. *Phys. Rev. X* **2018**, *8*, 041008. [CrossRef]
16. Dockx, K.; Cocolios, T.E.; Ferrer, R.; Granados, C.; Kraemer, S.; Kudryavtsev, Y.; Sels, S.; Van den Bergh, P.; Van Duppen, P.; Verlinde, M.; et al. A new control system for high-precision In-Gas Laser Ionization and Spectroscopy experiments at KU Leuven. *Nucl. Instrum. Methods Phys. Res. B* **2020**, *463*, 297–301. [CrossRef]
17. de Groote, R.P.; Verlinde, M.; Sonnenschein, V.; Flanagan, K.T.; Moore, I.; Neyens, G. Efficient, high-resolution resonance laser ionization spectroscopy using weak transitions to long-lived excited states. *Phys. Rev. A* **2017**, *95*, 032502. [CrossRef]
18. Varentsov, V. A New Approach to the Extraction System Design. In Proceedings of the SHIPTRAP Collaboration Meeting, Mainz, Germany, 19 March 2001. [CrossRef]
19. Brunner, T.; Fudenberg, D.; Varentsov, V.; Sabourov, A.; Gratta, G.; Dilling, J.; nEXO Collaboration. An RF-only ion-funnel for extraction from high-pressure gases. *Int. J. Mass Spectrom.* **2015**, *379*, 110–120. [CrossRef]
20. Querci, L.; Varentsov, V.; Günther, D.; Hattendorf, B. An RF-only ion funnel interface for ion cooling in laser ablation time of flight mass spectrometry. *Spectrochim. Acta B* **2018**, *146*, 57–68. [CrossRef]
21. Ratajczyk, T.; Bollinger, P.; Lellinger, T.; Varentsov, V.; Nörtershäuser, W. Towards a He-buffered laser ablation ion source for collinear laser spectroscopy. *Hyperfine Interact* **2020**, *241*, 52. [CrossRef]
22. Varentsov, V. *Review of Gas Dynamic RF-Only Funnel Technique for Ion Beams Cooling and Extraction into Vacuum*; FAIR: Darmstadt, Germany, 2022. [CrossRef]